NAVAL POSTGRADUATE SCHOOL
Monterey, California

THESIS

VOID FRACTION UNDER BREAKING WAVES

by

R.J. Piret

December 1999

Thesis Co-Advisors: Edward B. Thornton
Timothy P. Stanton

Approved for public release; distribution is unlimited.

REPORT DOCUMENTATION PAGE

Form Approved OMB No. 0704-0188

1. AGENCY USE ONLY *(Leave blank)*	2. REPORT DATE	3. REPORT TYPE AND DATES COVERED
	December 1999	Master's Thesis

4. TITLE AND SUBTITLE
VOID FRACTION UNDER BREAKING WAVES

5. FUNDING NUMBERS

6. AUTHOR(S)
Piret, Ronald J.

7. PERFORMING ORGANIZATION NAME(S) AND ADDRESS(ES)
Naval Postgraduate School
Monterey, CA 93943-5000

8. PERFORMING ORGANIZATION REPORT NUMBER

9. SPONSORING / MONITORING AGENCY NAME(S) AND ADDRESS(ES)

10. SPONSORING / MONITORING AGENCY REPORT NUMBER

11. SUPPLEMENTARY NOTES
The views expressed in this thesis are those of the author and do not reflect the official policy or position of the Department of Defense or the U.S. Government.

12a. DISTRIBUTION / AVAILABILITY STATEMENT
Approved for public release; distribution is unlimited.

12b. DISTRIBUTION CODE

13. ABSTRACT *(maximum 200 words)*

Bubble injection due to breaking waves within the surf zone is inferred by measuring void fraction using a 3 m vertical array of eight conductivity cells in conjunction with video pixel intensity. Void fraction errors associated with the conductivity measurements are examined, including vertical variations in the temperature and conductivity (measured), proximity effects near the surface, and estimates of the surface elevation using pressure sensors.

Energy loss is due to conversion of kinetic and potential energy of a wave to buoyant potential energy by the injection of air into the water column, which is then lost as the bubbles raise to the surface and escape to the atmosphere. Void fractions up to 40% were observed in intense breaking events penetrating to depths over 0.5 m confined within the crest-trough region. Production of potential energy due to buoyancy of bubbles was nearly instantaneous with the majority of energy dissipating within 0.25 s.

Pixel intensity qualitatively correlated with surface elevation and injection events. Crests in cross-shore intensity time stack plots are clearly visible and show good correlation with breaking events. However, pixel intensity values did not correlate quantitatively with surface elevation or production of buoyant potential energy.

14. SUBJECT TERMS	15. NUMBER OF PAGES
Bubble Injection, Void Fraction, Energy Dissipation, Video Pixel Intensity	52
	16. PRICE CODE

17. SECURITY CLASSIFICATION OF REPORT	18. SECURITY CLASSIFICATION OF THIS PAGE	19. SECURITY CLASSIFI- CATION OF ABSTRACT	20. LIMITATION OF ABSTRACT
Unclassified	Unclassified	Unclassified	UL

NSN 7540-01-280-5500

Standard Form 298 (Rev. 2-89)
Prescribed by ANSI Std. 239-18

Approved for public release; distribution is unlimited

VOID FRACTION UNDER BREAKING WAVES

Ronald J. Piret
Lieutenant, United States Navy
B.S., United States Naval Academy, 1993

Submitted in partial fulfillment of the
requirements for the degree of

MASTER OF SCIENCE IN METEOROLOGY AND PHYSICAL OCEANOGRAPHY

from the

NAVAL POSTGRADUATE SCHOOL
December 1999

Author: _____
Ronald J. Piret

Approved by: _____
Edward B. Thornton, Thesis Co-Advisor

_____
Timothy P. Stanton, Thesis Co-Advisor

_____
R.W. Garwood, Chairman
Department of Oceanography

ABSTRACT

Bubble injection due to breaking waves within the surf zone is inferred by measuring void fraction using a 3 m vertical array of eight conductivity cells in conjunction with video pixel intensity. Void fraction errors associated with the conductivity measurements are examined, including vertical variations in the temperature and conductivity (measured), proximity effects near the surface, and estimates of the surface elevation using pressure sensors.

Energy loss is due to conversion of kinetic and potential energy of a wave to buoyant potential energy by the injection of air into the water column, which is then lost as the bubbles raise to the surface and escape to the atmosphere. Void fractions up to 40% were observed in intense breaking events penetrating to depths over 0.5 m confined within the crest-trough region. Production of potential energy due to buoyancy of bubbles was nearly instantaneous with the majority of energy dissipating within 0.25 s.

Pixel intensity qualitatively correlated with surface elevation and injection events. Crests in cross-shore intensity time stack plots are clearly visible and show good correlation with breaking events. However, pixel intensity values did not correlate quantitatively with surface elevation or production of buoyant potential energy.

TABLE OF CONTENTS

LIST OF FIGURES

I. INTRODUCTION

As a wave breaks, the plunging jet injects air into the water column converting potential and kinetic energy of the wave into turbulent kinetic energy and potential energy in the form of buoyant air bubbles. These bubbles then rise to the surface and burst, releasing their energy into the atmosphere. The objective of this paper is to measure the dissipation of wave energy due to entrainment of air during wave breaking and relate the amount of dissipation to wave breaking parameters and the optical brightness of the surface.

The depth and distribution of bubble injection events have been measured using various techniques in both saltwater and freshwater environments including: UV light sources with fluorescent particles, He-Ne lasers, video and still photography as well as impedance and conductivity sensors. These techniques work well in the controlled environment of a wave tank. However, it is difficult *in-situ* to position sensors just below the surface of a bubble injection event. Relying on single sensors in a fixed location can lead to infrequent observations of substantial injection events.

Previous studies of void fraction can be divided into shallow water and deep water breaking. Wave breaking and bubble entrainment inside the surf zone were first studied by Horikawa and Kuo (1966). They observed that air entrainment associated with turbulence generated by a breaking wave is significant to energy dissipation.

Fuhrboter (1970) hypothesized that the sudden reduction of wave height and wave energy could be explained by air entrainment. However, Fuhrboter conceded that the concentration and distribution of air entrainment was nearly unknown owing to a lack of *in situ* observations. Fuhrboter assumed uniform concentration of bubbles dissipated within one wavelength, postulating that the turbulent layer was advected along with the wave front.

Koga (1981) employed an overlapping exposure photographic technique to measure air entrainment in breaking wind waves in a tank. He noted that initial entrainment was caused by an ordered downward flow on the leading slope of the wave.

Jansen (1986) disagreed with Fuhrboter's advection of the turbulent layer along the wave front, but supported Koga's observation of ordered downward flow. He determined that horizontal wave momentum at breaking is transformed to

form a jet. The jet is nearly free falling downward momentum, entraining air into the water column. Small-scale turbulence is generated by the interaction of jet splashes on the wave front. He employed UV light sources with near neutrally buoyant fluorescent particles to track injection events (for shallow water breaking waves in a fresh water wave tank). On a uniformly sloped beach (β= 1:30) several jet splashes were observed on the front of a plunging breakers. Each jet splash resulted in an injection event further complicating relationships between wave attenuation, bubble distribution and energy dissipation. Jansen observed that for plunging waves the first two jet splashes, accounted for 20-25% each of the total wave energy dissipation, while subsequent injections accounted for 10-15% each of the total wave energy dissipation.

Hwung, Chyan and Chung (1992) theorized that at the instant of wave breaking in shallow water, air entrainment destroys the original flow, resulting in dissipation of wave energy. They employed a He-Ne laser and 2D LDV in a fresh water wave tank to investigate characteristics of bubble concentration, depth of penetration and velocity fields. They found for monochromatic waves of varying

steepness and bed slopes that the concentration of bubbles decays exponentially in the vertical. The kinetic energy increased slightly between the impinging point and the depth of maximum penetration. In this region, the loss of potential and kinetic energy are attributed to air entrainment. They concluded that concentration of air bubbles decays exponentially in the vertical for both plunging and spilling breakers.

Lamarre and Melville (1991,1992) measured void fraction with conductivity probes for deep water plunging waves in laboratory and field experiments. They found that void fraction was dependent on significant wave height and wind speed for deep water breaking waves. Nearly 30-50% of total energy dissipation can be attributed to air entrainment in plunging breakers.

Loewen et al. (1996) studied void fraction in deep water spilling waves using a video camera and a back lighting technique to analyze size distributions of large bubbles in freshwater and saltwater wave tanks. They confirmed that for the sensor void fraction, bubbles are smaller in saltwater compared with freshwater. Salt water residency times were also found to be longer due to buoyancy and frictional effects of the smaller bubbles.

This difference in bubble size distribution was thought to have an impact on injection patterns, distributions and energy dissipation. They calculated the energy required to submerge bubbles as a function of size to various depth. Based on this analysis the energy dissipation due to air entrainment of measured bubble size distribution and concentration were calculated, finding values of 0.05-0.4% for spilling breakers. This is much smaller than the 30-50% Lamarre and Melville calculated for plunging breakers. Loewen et al. attribute some of the difference to the type of breakers observed.

Slauenwhite and Johnson (1999) compared bubble production in fresh and salt water. They found that bubble production was not simply a matter of surface tension, viscosity, density or ionic strength, but also factors they were unable to determine.

Gemmrich (1992) used four conductivity cells in a vertical array, suspended from a floating platform, to obtain void fraction in open ocean breaking waves. He found that for the 11 s peak wave period the average void fraction event of 10% lasted only 0.5 s, while void fraction events greater than 40% lasted on the order of 1.3 s. Su and Cartmill (1993) attained qualitatively similar

results utilizing resistive gauges suspended from a tethered float.

In this paper, the volume of bubbles (void fraction) is inferred by measuring the change in conductivity of the water/air mixture. Void fraction is used to calculate the potential energy of entrained air, which is compared with optical brightness of the surface. Conductivity measurements were acquired in the nearshore during the SandyDuck97 experiment using a 3 m vertical array of eight conductivity sensors. In the following sections, a description of the SandyDuck97 experiment, methodology, theory, results and conclusions are presented.

II. EXPERIMENT

The measurements used in this analysis are part of a comprehensive nearshore experiment, SandyDuck97, conducted at the U.S. Army Corps of Engineers Field Research Facility (FRF) on the Outer Banks at Duck, North Carolina. The beach is a two-bar system with a dynamic inner bar (30-120 m offshore) and a secondary bar with lower amplitude (300-400 m offshore). The mean foreshore slope of the beach is ~0.08 (1:12), and the slope offshore of the bars is ~0.006 (1:170) [Lippman et al., 1993]. Measurements were taken from late September to early November.

A specially designed sled was built as a platform for a variety of sensors (Figure 1). The sled was 3 x 4 m, constructed of 6 inch aluminum pipe frame with two 5 m, 20 cm diameter runners. An array of eight FSI conductivity sensors was mounted on a 3 m steel pole. The sensors were positioned approximately 0.3 m apart from the top down with an eighth sensor near the bottom acting as a reference. The sensors were tilted upward at 45° toward the impinging wave. (Figure 2). The 45° upward tilt allows bubbles to escape without being trapped within the .0165 m diameter cylinder, which comprises the sensor head (Figure 3).

Surface elevation was measured using a Hydracon strain gage pressure sensor mounted on the sled directly below the conductivity array at an elevation of 0.25 m above the bed.

All data acquired on the sled was digitized at 48.2303 Hz *in-situ* and transmitted back to shore via a fiber-optic cable where they were recorded.

Video data, courtesy of Professor Tom Lippman of Ohio State University, was used to establish breaking events and their relative position to the conductivity array. Cameras were mounted on top of a 44 m tower in weatherproof housings and hard wired to the FRF building for recording. Video data were recorded continuously throughout the experiment encompassing the sled track.

CTD profiles taken at the end of FRF pier were used to measure density profiles. Data analyzed are limited to days when the water column was well-mixed with no significant temperature or salinity gradients (i.e. the bulk conductivity of the water was uniform with depth).

The sled was initially positioned offshore by the 11 m high Coastal Research Amphibious Buggy (CRAB) pictured with the sled in Figure 1. CRAB positions were determined by differential GPS. The sled was sequentially pulled shoreward to various cross-shore positions. One-hour of

data was recorded at each station. Five to eight stations were recorded along the FRF transect 935 m north of the FRF pier.

THIS PAGE INTENTIONALLY LEFT BLANK

III. THEORY

Air in salt water, measured as void fraction, decreases the measured conductivity. Maxwell (1891) derived an expression for the effective conductivity of a heterogeneous medium, σ_{eff} dispersed in an ambient medium of conductivity σ_w. In our experiments, σ_{eff} is the measured conductivity including submerged bubbles:

$$\sigma_{eff} = \frac{(1 - \alpha)}{(1 + \alpha/2)} \sigma_w \qquad (1)$$

where α is the volumetric fraction occupied by the entrained air. The ambient conductivity σ_w of saltwater is measured with the bottom reference sensor, where it is assumed that the bubbles do not penetrate to the bottom and that the conductivity in the absence of bubbles is uniform with depth. Solving for void fraction:

$$\alpha = \frac{2(1 - \sigma_{eff}/\sigma_w)}{(2 + \sigma_{eff}/\sigma_w)} \qquad (2)$$

For the case of the sensor coming out of the water, the effective conductivity σ_{eff} goes to zero and void fraction approaches one.

The potential energy per unit area due to air entrainment can be calculated by integrating the depth of penetration of void fraction over the vertical:

$$E_b(t) = \rho g \int_{-h}^{\eta} \alpha(z,t)\, z\, dz \qquad (3)$$

where the buoyancy anomaly $\rho g \alpha(z,t)$ of the entrained air is multiplied by the depth below the surface z.

The rate of potential energy production and subsequent dissipation, owing to air entrainment, is calculated by differentiating $E_b(t)$ with respect to time:

$$\varepsilon_b(t) = \frac{dE_b}{dt} \qquad (4)$$

The energy dissipation due to air entrainment, $\langle \varepsilon_b \rangle$, is compared with the total wave energy.

IV. ANALYSIS

Data sets, approximately one-hour in length, acquired on 16 and 21 October 1997 are analyzed. The data sets were chosen for presence of energetic breaking events and sufficient depth of water for the reference sensor to remain unaffected by bubbles. The water temperature ranged between 19 and 21 degrees Celsius. Tides at Duck, NC are semidiurnal. Wind speeds on 16 October 1997 reached as high as 10 m/s with significant wave heights of 1.65 m. Wind speed decreased on 21 October below 5 m/s with significant wave heights of 1.72 m.

Surface elevation is determined from the measured pressure data. The pressure signal was first detrended before Fourier transforming the selected data. The linear wave theory spectral transformation function:

$$H(f) = \frac{\cosh(KH)}{\cosh(K(H-Z))} \tag{5}$$

was applied to the complex Fourier amplitudes in the frequency domain, and then inverse transformed to calculate surface elevation time series (Guza and Thornton, 1980). The data were then low pass filtered to remove high frequency noise.

Assuming wave heights are Rayleigh distributed, the rms wave height is calculated:

$$H_{rms} = 8^{1/2} \ (\sigma_\eta)^{1/2} \tag{6}$$

where σ_η is the standard deviation of surface elevation. Total wave energy is calculated using linear wave theory:

$$E = 1/8 \ \rho g \ H_{rms}^2 \tag{7}$$

Potential energy due to air entrainment is calculated from the void fraction profiles, measured using the vertical array of eight conductivity sensors. Conductivity can vary owing to variations of temperature, salinity and void fraction. Variations in conductivity due to temperature and salinity over the vertical are eliminated by normalizing the top seven sensors with the bottom sensor. This assumes the temperature and salinity are homogeneous over the vertical. CTD profiles taken at the end of the FRF pier assured a well-mixed water column with no significant temperature or salinity gradients on the days considered for analysis. The bottom sensor was completely submerged for the analyzed data and did not experience any bubble injection events, thereby acting as a maximum value for each time step.

Conductivity values are affected by proximity of the sensor to the air/water interface, initial displacement

(wake effect), and finite sensor frequency response when entering the water. Conductivity decreases as the probe approaches the surface owing to distortion of the inductive field, resulting in false void fractions. In the laboratory the conductivity sensor was incrementally raised toward the surface in a well-mixed bath of constant and homogenous temperature and salinity. Measurable conductivity changes occurred when the sensor was within 0.1 m of surface (Figure 4).

The response of the conductivity sensor was measured by selecting data when the probe was passing in and out of the water for non-breaking wave cases, such that the void fraction is assumed zero within the water. The sensor response (measured at e^{-1}) was 0.13 s upon entering the water (Figure 5), slower than the 0.03 s response upon exiting the water (Figure 6).

A wake effect may also occur because of the sensor's finite size. The wake effect causes lowering of initial conductivity values as the sensor transits through the wave surface momentarily displacing water before becoming enveloped. This may be the reason for the slower measured response on entering the water compared with exiting the water.

As a result of these effects, conductivity measurements taken near the surface can return false void fractions. By gating the data near the surface and within the base sensor frequency response, false void fractions can be avoided. A two-fold gate was applied to the data accounting for increased void fractions caused by proximity to the surface and finite sensor frequency response. The time constant .13 s illustrated in figure 5 was applied to selected data when the sensor was entering the water. This process removed false measurements caused by finite sensor response and wake effect. The second gate was applied to cases where the sensor was exiting or nearing the surface. Sensors heights were also adjusted to account for the tilt of the sled on uneven bedforms.

Precise knowledge of the surface elevation is required to know when the sensors are coming in and out of the water. If the conductivity sensor is incorrectly indicated to be in the water, a large error in void fraction occurs. The surface elevation was determined by transforming the pressure signal using a linear wave theory transformation function. Errors are introduced by not including nonlinearities of the transformation. For this reason data acquired within 0.1 m of the surface were not included.

Therefore, the void fraction estimates are conservative (underestimates).

THIS PAGE INTENTIONALLY LEFT BLANK

V. RESULTS

The energy spectrum of the surface elevation at the vertical array (Figure 7) shows a relatively narrow spectrum with a peak frequency at .09 Hz. The root mean square wave height was 1 m (10.7 s period). The mean wave angle of approach at 8 m was 2 degrees.

The beach profile for SandyDuck 97 varied from previous years with a less defined inner bar. This created a narrow and yet ill defined surf zone in relatively shallow water. This presented difficulties insuring the reference sensor was in water deep enough to remain unaffected by injection events, and that the sled was positioned within the surf zone. The sled was positioned, for the analyzed data, on the outer edge of the surf zone where breaking was intermittent. Winds in excess of 10 m/s increased remnant foam on the surface through the process of micro-breaking. Decreased variance in the pixel intensity made distinction of individual breaking events difficult.

The top seven sensors on the conductivity array were normalized by the bottom sensor to account for effects of changing bulk temperature and salinity over time. The data set was examined to assure the bottom sensor was unaffected

by intense injection events and remained at its peak value throughout data runs.

Data chosen for analysis were acquired on 16 October 1997 when the sled was stationed on the outer edge of the surf zone such that the upper sensors were coming in and out of the water. During most of the breaking wave events analyzed, sensor 6 is very near the surface and is essentially discarded (Figure 8). Also some of the resident bubbles at the immediate surface of the water are due to the advection of bores and are eliminated from the true bubble injection. Sensors 4 and 5 are within 0.5 m of the surface and return expected conductivity data. At 0.5 m below the surface, sensor 3 conductivity generally remains unaffected by injection events. Therefore, at this location the depth of penetration of bubbles was confined within the crest-trough region of the waves.

Void fraction is calculated using Equation 2 using the conductivity measurements over one hour. Void fractions as large as 40% were observed. Examination of the data found that even in the most intense injection events residence times lasted no more than 1.5 s.

Potential energy due to bubble injection and energy production/dissipation rate is shown with surface elevation

in Figure 9. Peak values of potential energy due to bubble injection are nearly instantaneous and quickly return to zero as bubbles raise to the surface within one second in most cases—less than 15% of the mean period of the waves.

Maximum values of potential energy (E_b) peaked at nearly 4000 joules/m^2 and coincide with the peaks in the water elevation. The majority of potential energy is dissipated within 0.25 s. Since duration of dissipation was usually no more than 1.5 s, we observed buoyant potential energy dissipation at rates of 2700 joules/s. These results qualitatively agree with Gemmrich who observed time of energy dissipation between 0.5-1.35 s.

Variations of the proximity filter from 0.1 m to 0.05 m were applied to the conductivity data. Potential energy production increased less than 1% over the one hour of data indicating that the analysis is not sensitive to masking the upper 0.1 m. Potential energy is the product of void fraction and distance beneath the surface (Equation 2). Therefore, variations in void fraction near the surface result in insignificant values of potential energy compared to the overall potential energy production.

Pixel intensity data was used to help identify breaker lines and types of breakers. Time stacks of pixel

intensity in the cross-shore on the same line as the sled are shown in Figure 10. Using time stacks, breaking waves can be identified by the increased pixel intensity shown as white crests in the cross shore field. The breaking events are easily identified and qualitatively correspond to potential energy events. However, pixel intensity does not correlate with surface elevation or potential energy production with maximum correlation values of 0.12 and 0.28 calculated from the cross-correlation function (Figures 11 and 12). An apparent time offset of nearly two seconds exists between wave breaking events and peaks in pixel intensity. Bubbles advected along the wave front may account for a portion of the lead, but uncertainty in the time base itself is unresolved.

Comparatively good correlation exists between surface elevation and injection events of void fraction with a maximum value of .65 (Figure 13). Maximum values in buoyant potential energy lag peak values in surface elevation by .15 s.

VI. CONCLUSIONS

The potential energy production during wave breaking events due to bubble injection was measured as void fraction by conductivity sensors. The potential energy is compared with surface elevation and optical brightness at the surface. Accurate determination of the surface elevation with respect to sensor height was found to be critical to accurate measurement of void fraction. Errors in void fraction as small as 1% (due to sensor proximity to the wave surface) can result in errors greater than 10% in potential energy production.

Void fractions up to 40% were observed in intense injection events penetrating to depths of over 0.5 m confined within the crest-trough region. Potential energy production due to buoyancy of the bubbles was nearly instantaneous with the majority of energy dissipating within 0.25 s. Even in the most intense injection events, resident time of bubbles lasted no more than 1.5 s, well within 15% of the mean wave period.

Pixel intensity qualitatively correlated with surface elevation and injection events. Crests in the time stack plots are clearly visible and show good correlation with breaking events. However, quantitatively pixel intensity

values did not correlate well with surface elevation or production of buoyant potential energy.

This research is ongoing and data sets are being sought where conductivity sensors are well within the surf zone where pixel intensity and wave heights are expected to have higher correlation.

There are many difficulties encountered positioning sensors in-situ for void fraction observations. Relating relative brightness values of pixel intensity to breaking events could allow void fraction to be measured remotely. This method is relatively inexpensive and avoids the difficulties of placing sensors in the surf zone. This could also result in longer data sets acquired at less cost.

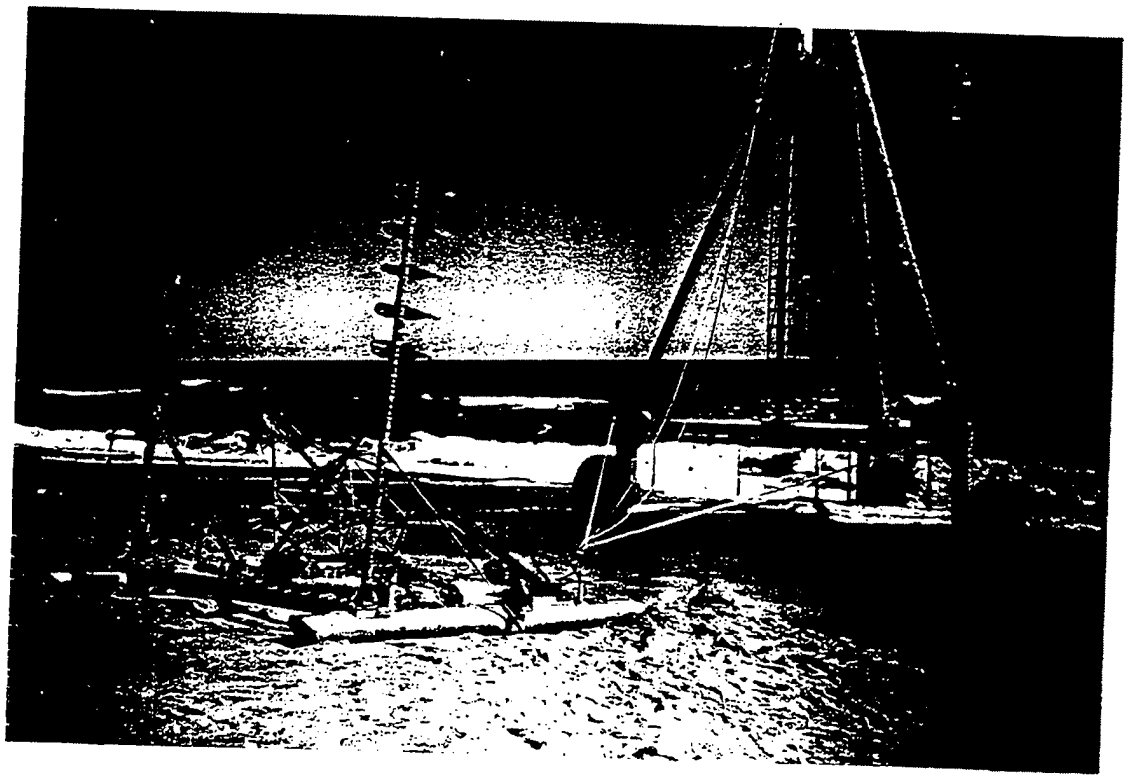

Figure 1. Photo of Sled and Vertical Conductivity Array towed by CRAB at Duck, NC, 1997

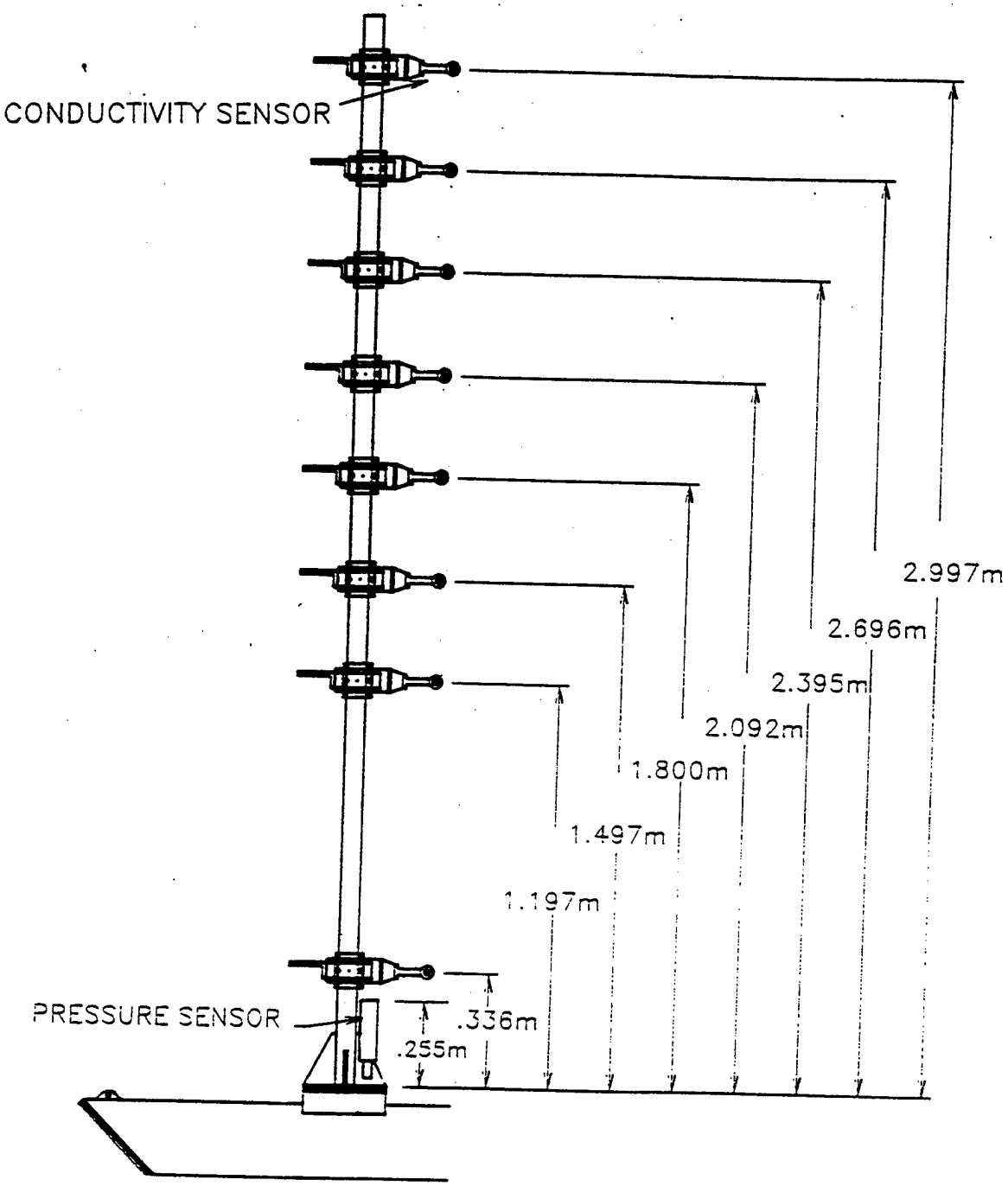

Figure 2. Schematic of the Vertical Array Showing Location of Conductivity and Pressure Sensors

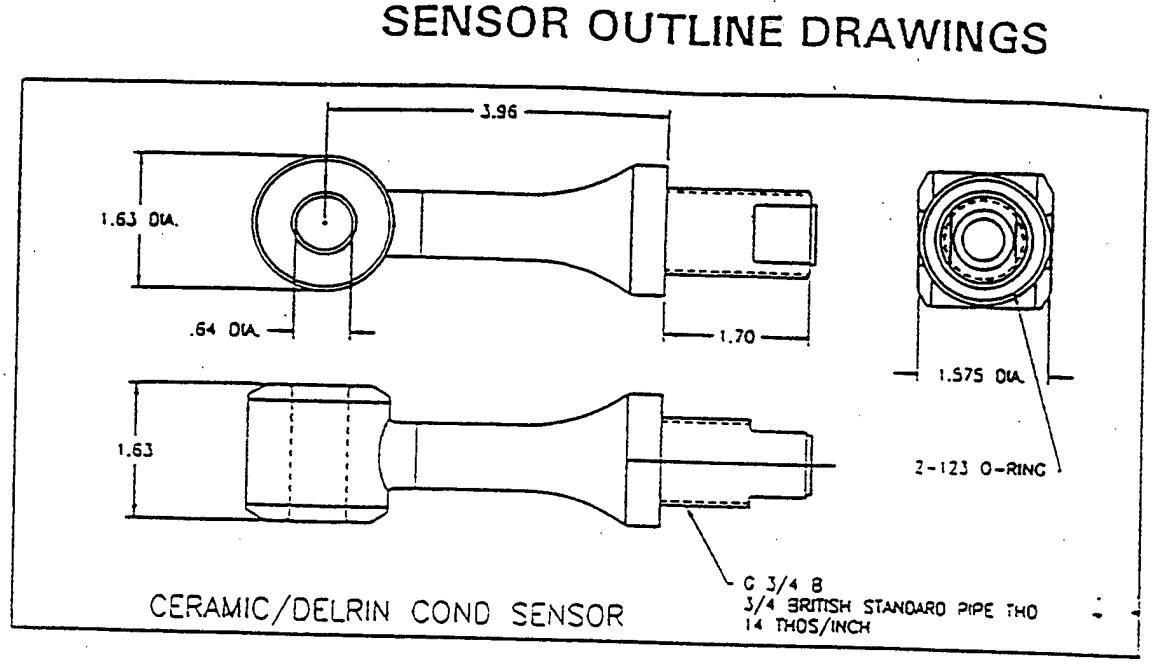

Figure 3. FSI Conductivity Sensor

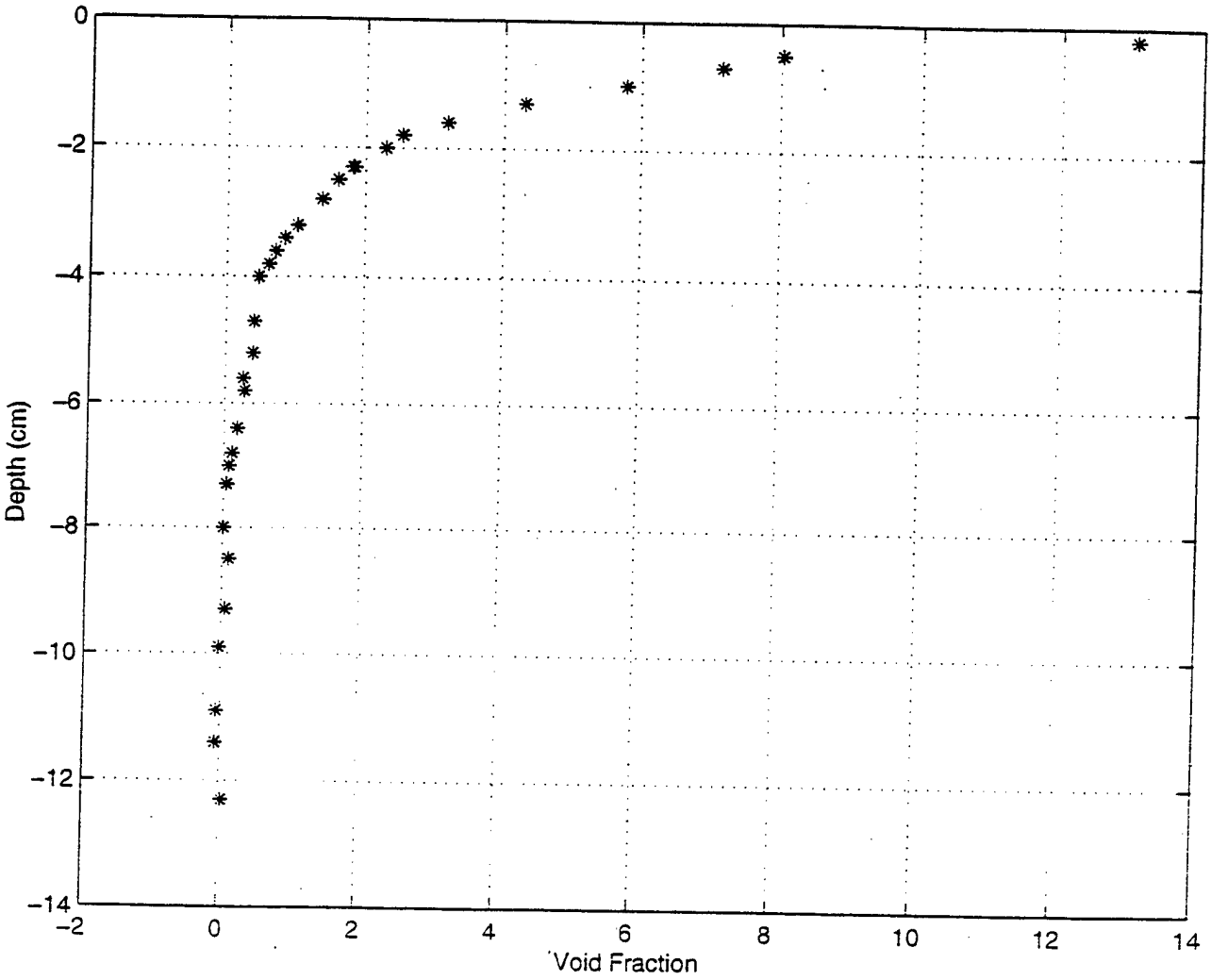

Figure 4. Proximity of Sensor to Water Surface Increases Apparent Void Fraction Due to Distortion of Inductive Field

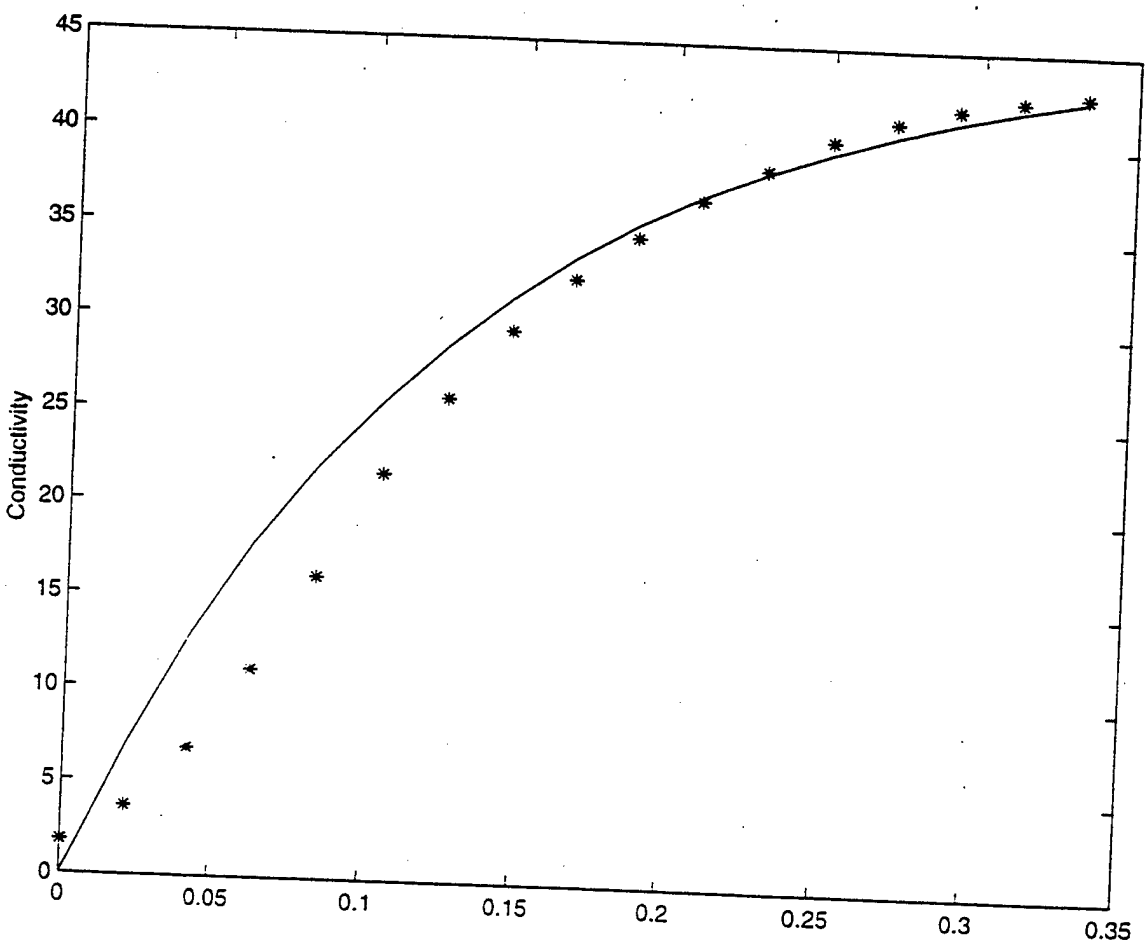

Figure 5. Frequency Response of Conductivity Sensor Entering Water

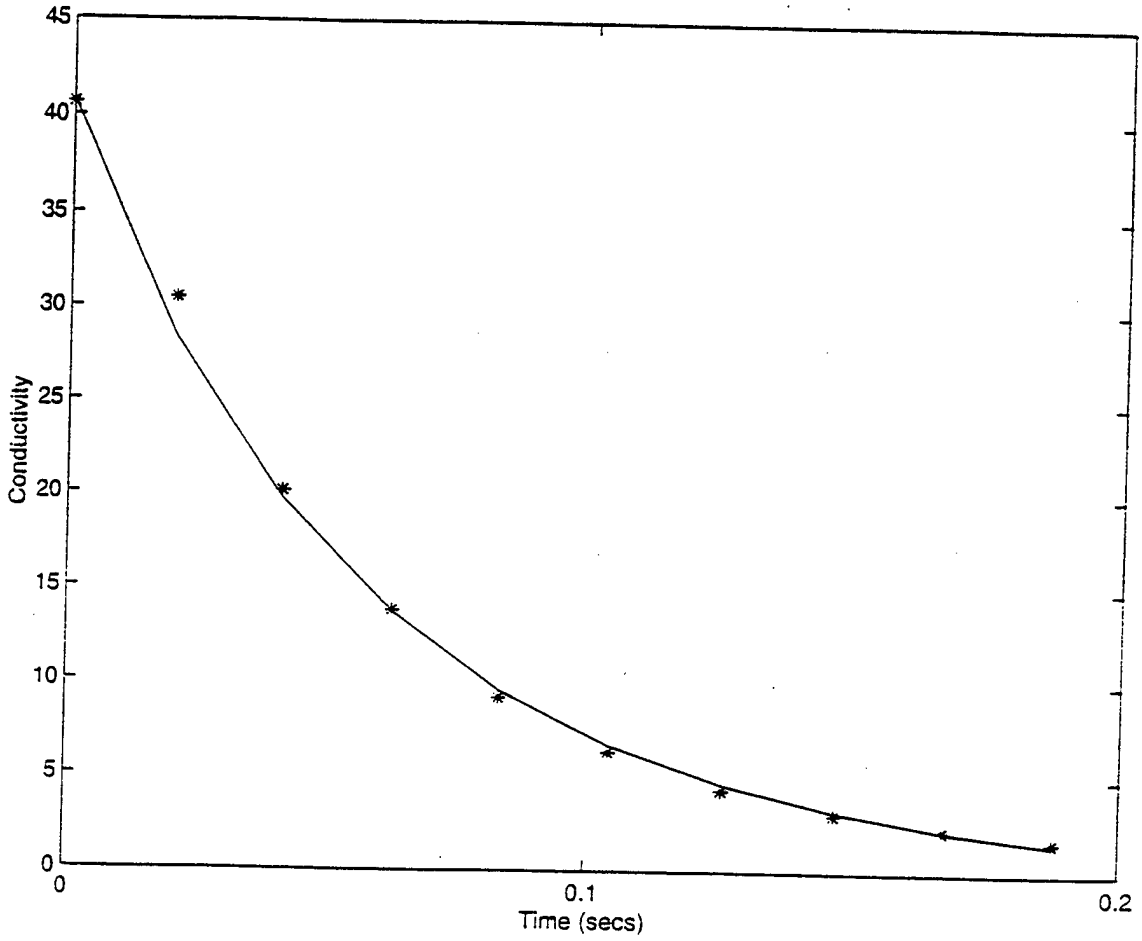

Figure 6. Frequency Response of Conductivity Sensor Exiting Water

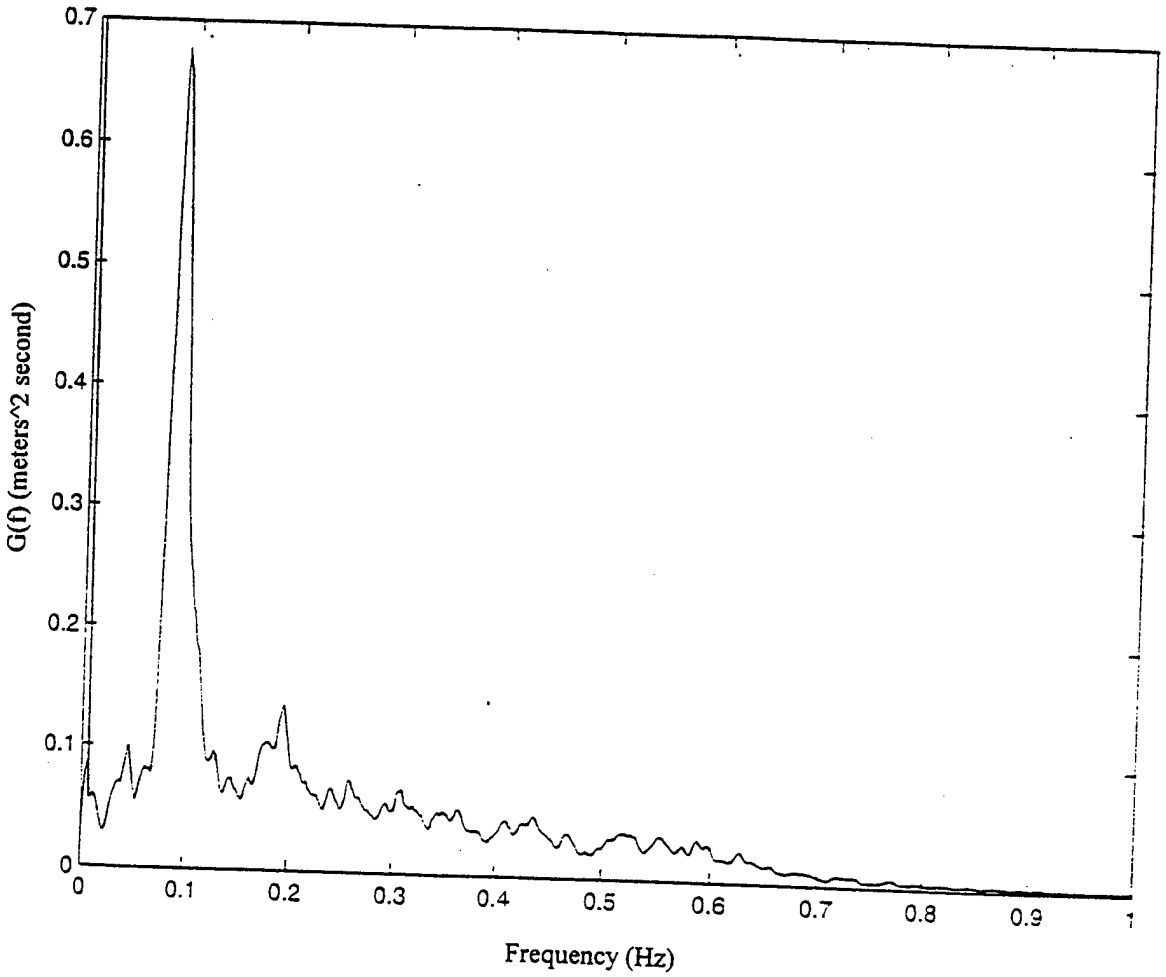

Figure 7. Energy Spectrum of Water Surface Elevation vs. Frequency

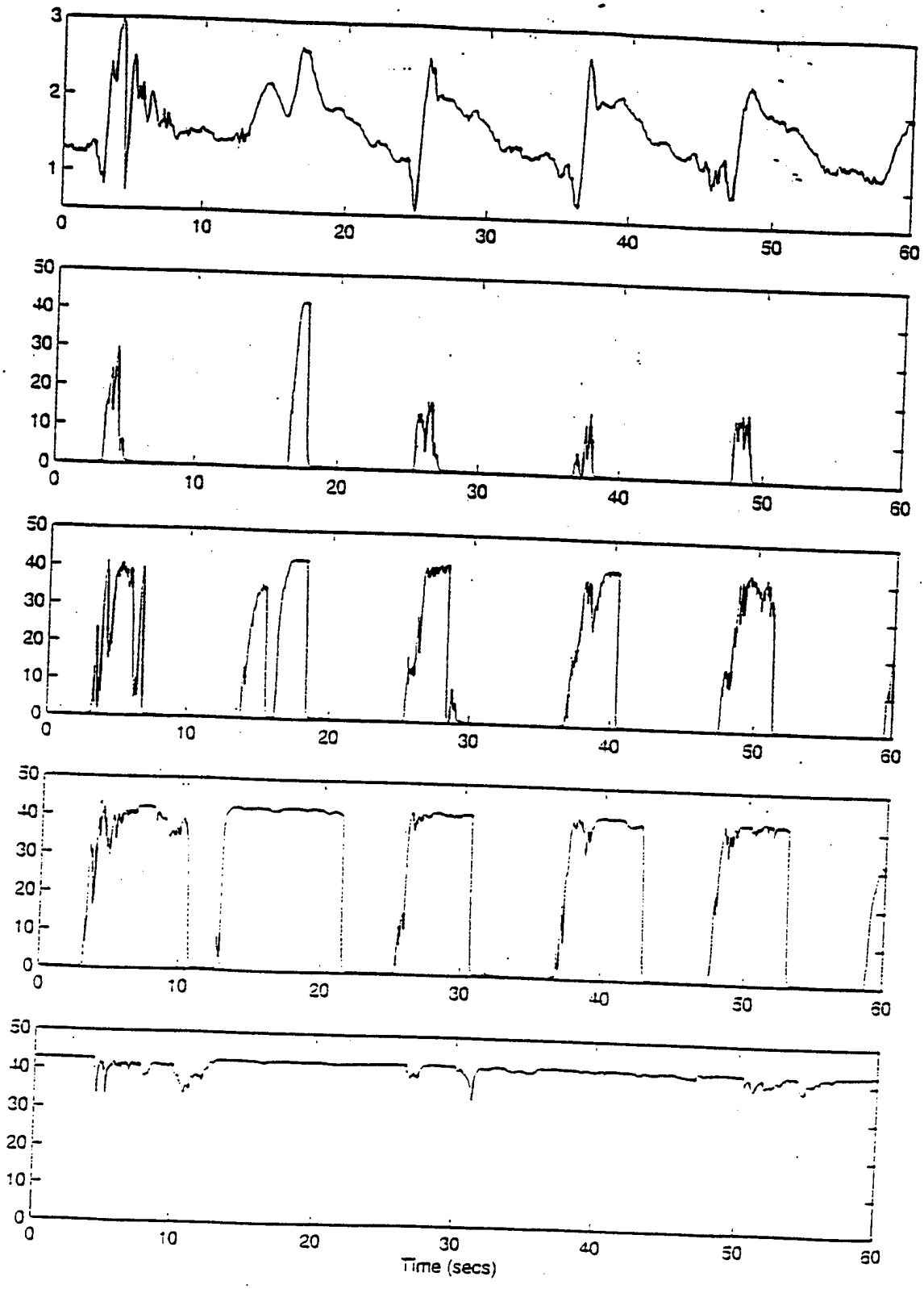

Figure 8. Conductivity Sensors 6,5,4 and 3 and Water Surface Elevation vs. Time

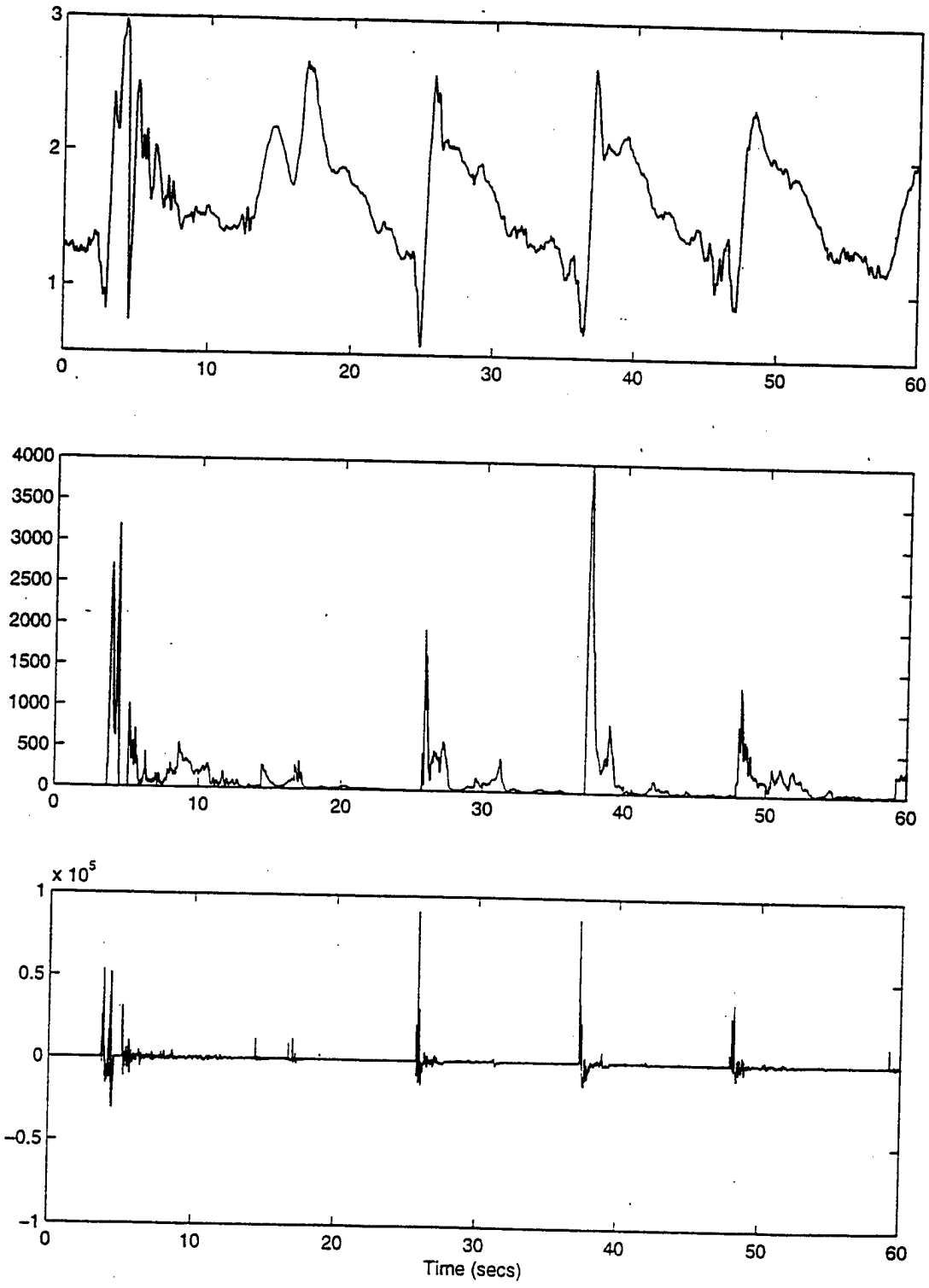

Figure 9. Water Surface Elevation (upper), Bubble Potential Energy (center), and Rate of Bubble Potential Energy Change (lower) vs. Time

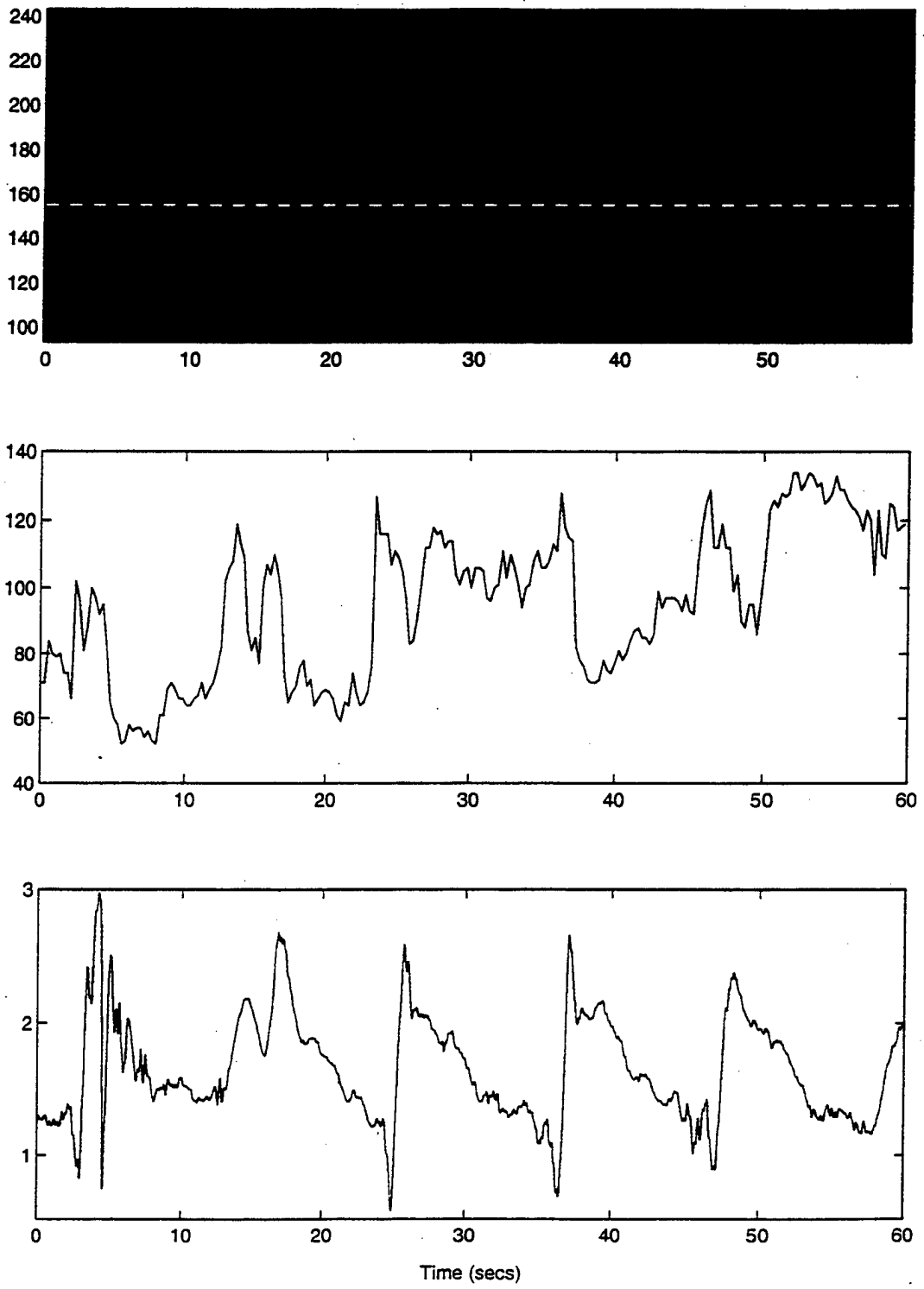

Figure 10. Time Stack (upper), Video Pixel Intensity (center), and Water Surface Elevation (lower) vs. Time

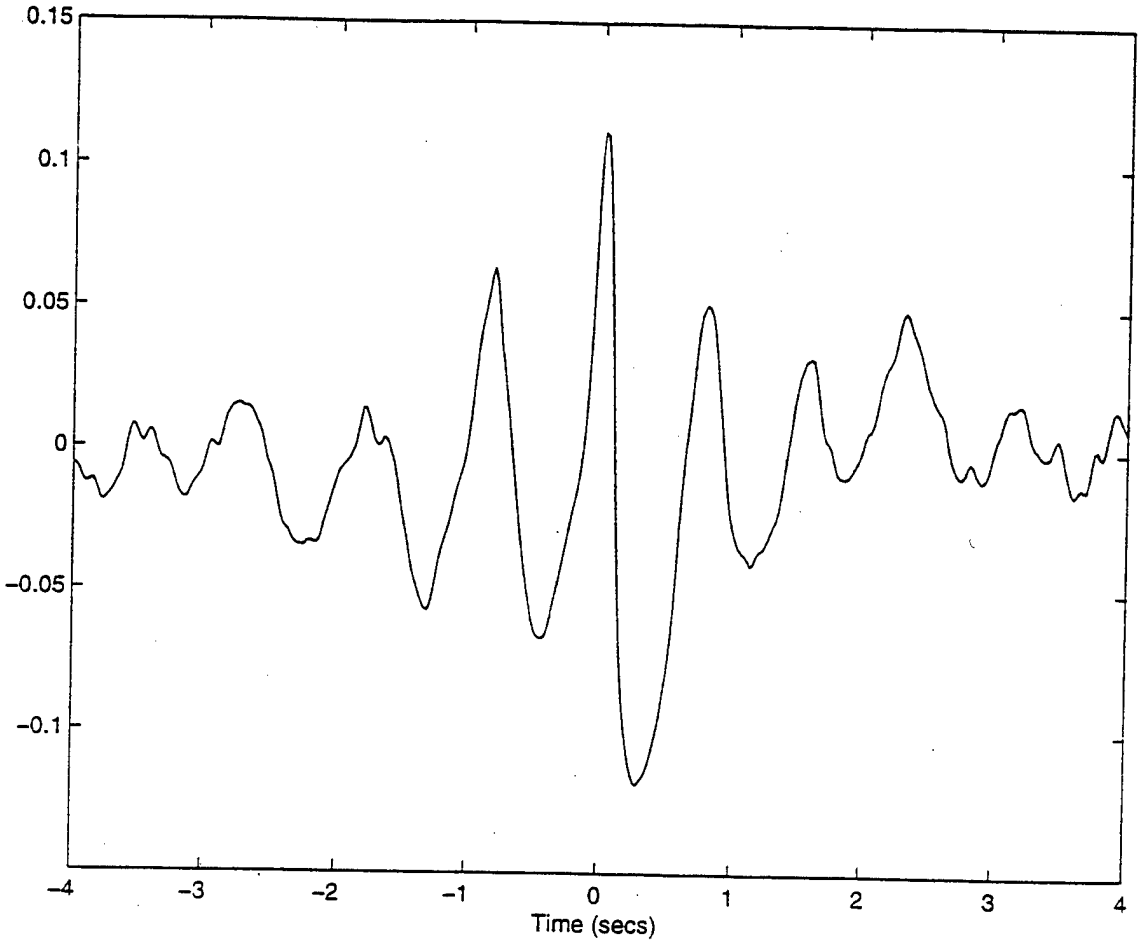

Figure 11. Correlation Function of Video Pixel Intensity and Water Surface

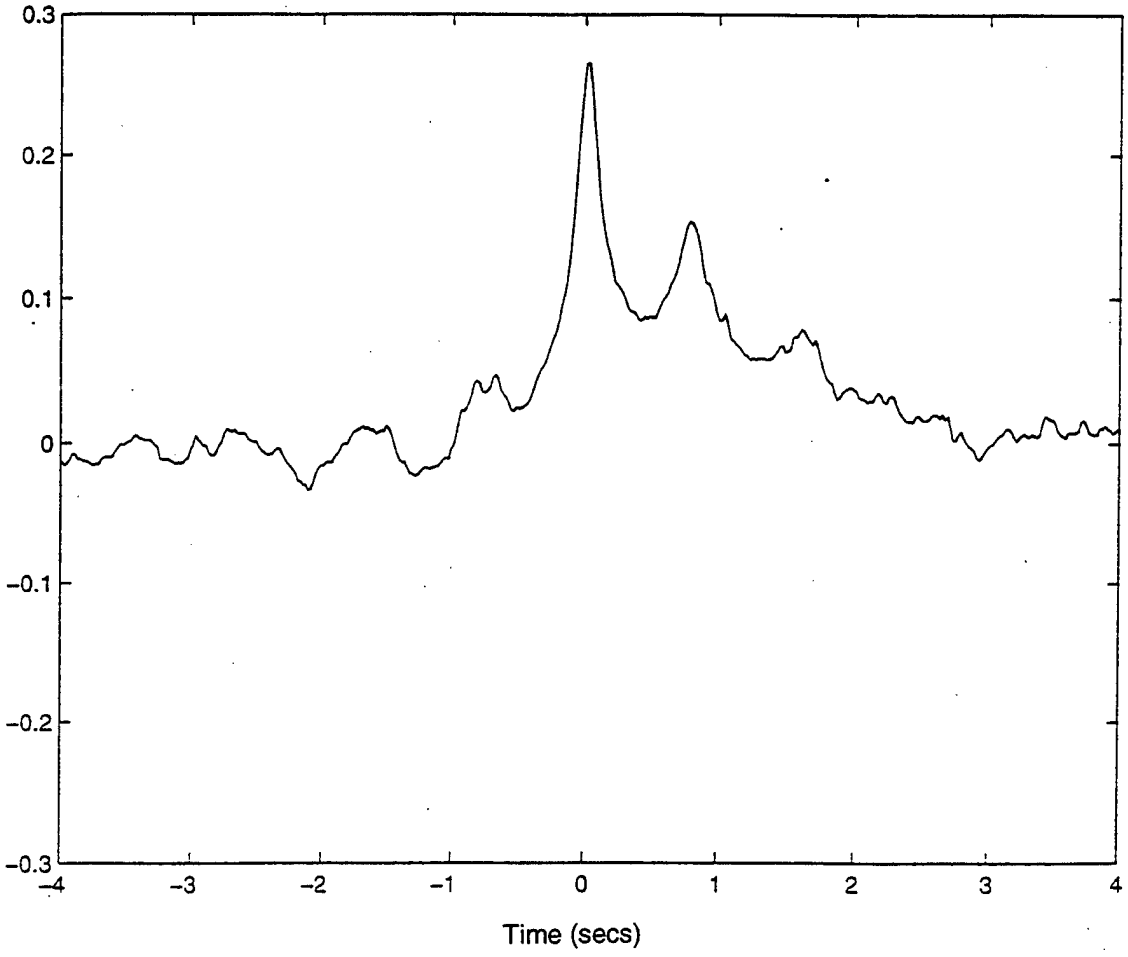

Figure 12. Correlation Function of Video Pixel Intensity and Bubble Injection Events

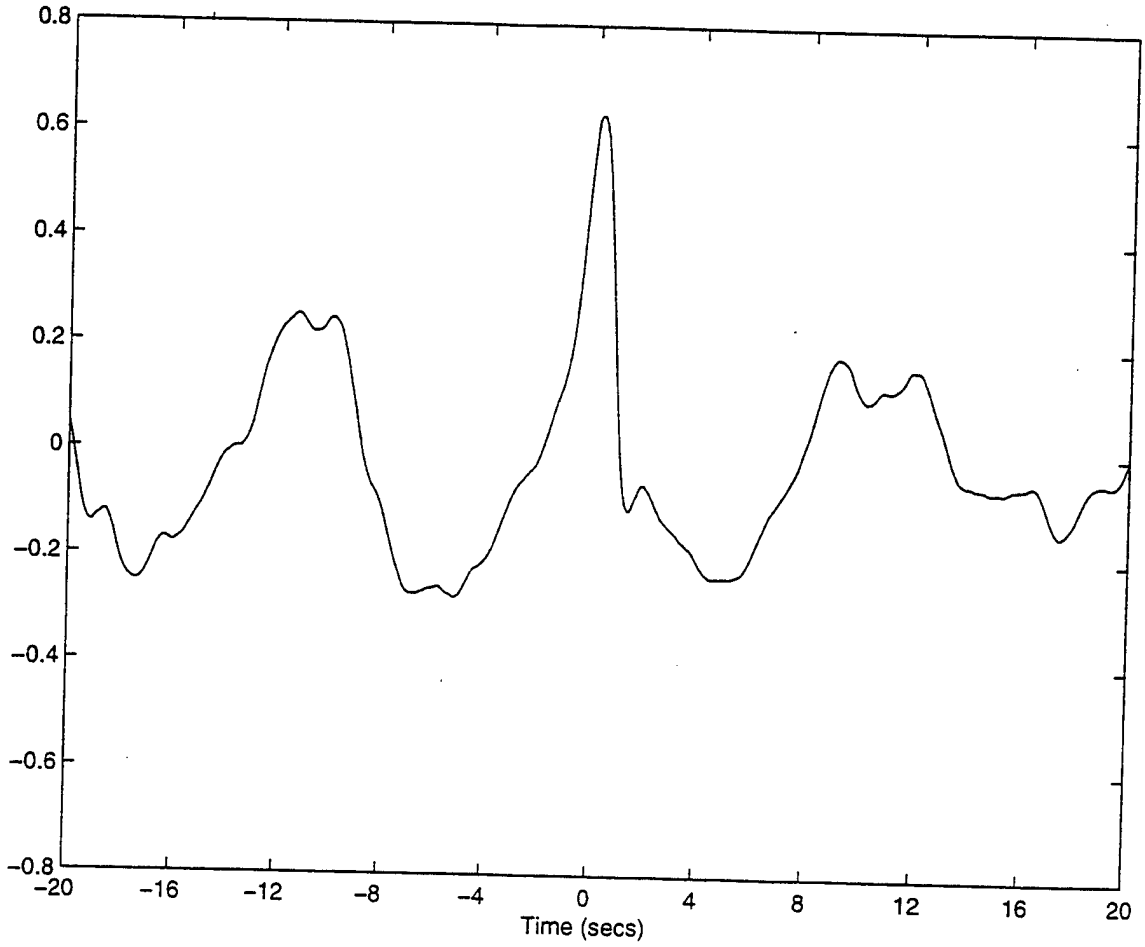

Figure 13. Correlation Function of Water Surface Elevation and Bubble Injection Events

THIS PAGE INTENTIONALLY LEFT BLANK

LIST OF REFERENCES

Fuhrboter, A., 1970, Air Entrainment and Energy Dissipation in Breakers, in *Proc. 12th Conf. On Coastal Eng.*, 319-398

Gemmich, J., 1992, Characteristics of Breaking Waves as Observed by the Drifter Flex, in *Proc. First Intl. Symp. Ocean Wave Meas. And Anal.*, 963-974

Guza, R. and E.B. Thornton, 1980, Local and Shoaled Comparisons of Sea Surface elevations, Pressures, and Velocities, *J. Geophys. Res., 85,3,* 1524-1530

Horikawa, K. and C.T. Kuo, 1966, A Study of Wave Transformation Inside Surf Zone, in *Proc. 4th Conf. On Coastal Eng.,* 217-233

Hwung, H.H., J.M. Chyan, and Y.C. Chung, 1992, Energy Dissipation and Air Bubbles Mixing Inside the Surf Zone, in *Proc 23rd International Conf. On Coastal Eng.*, 308-321

Jansen, P.C.M., 1986, Laboratory Observations of the Kinematics in the Aerated Region of Breaking Waves, *Coastal Eng.*, 9, 453-477

Koga, M., 1982, Bubble Entrainment in Breaking Wind Waves, *Tellus,* 34, 481-489

Lamarre, E. and W. Melville, 1992, Instrumentation for the Measurement of Void-Fraction in Breaking Waves: Laboratory and Field Results. *IEEE Journal of Ocean Engineering, 17(2),* 204-215

Lamarre, E. and W. Melville, 1991, Air Entrainment and Dissipation in Breaking Waves. *Nature,* 315, 469-472

Lippman, T.C., R.A. Holman, and K.K. Hathaway, 1993, Episodic, Non-Stationary Behavior of a Double Bar System at Duck, North Carolina, U.S.A., 1986-191991, *J. Coastal Res.*, 15, 49-75

Loewen, M.R., M. O'Dor, and M. Skafel, 1996, Bubbles Entrained by Mechanically Generated Breaking Waves. *J. Geophys. Res.*, 101, 20759-769

Maxwell, J.C., 1891, A Treatise on Electricity and Magnetism. Dover, 314

Slauenwhite, E., and B.D. Johnson, 1999, Bubble Shattering: Differences in Bubble Formation in Fresh Water and Sea Water. *J. Geophys. Res.*, 104, 3265-275

Su, M.Y., and J. Cartmill, 1993, Breaking Wave Measurement by a Void Fraction Technique, in *Proc. Second Intl. Symp. Ocean Meas. And Anal.*, 951-962

Thornton, E.B. and R. Guza, 1980, Transformation of Wave Height Distribution, *J. Geophys. Res., 88,10,* 5925-5938

INITIAL DISTRIBUTION LIST

1. Defense Technical Information Center.....2
   8725 John J. Kingman Road
   STE 0944
   Fort Belvoir, VA 22060-6218

2. Dudley Knox Library.....2
   Naval Postgraduate School
   411 Dyer Road
   Monterey, CA 93943

3. Chairman, Department of Oceanography.....1
   Code OC/Bo
   Naval Postgraduate School
   Monterey, Ca 93943

4. Dr. E.B. Thornton.....2
   Code OC/TM
   Oceanography Department
   Naval Postgraduate School
   Monterey, Ca 93943

5. Timothy P. Stanton.....2
   Code OC/ST
   Oceanography Department
   Naval Postgraduate School
   Monterey, CA 93943

6. LT R.J. Piret.....2
   567 Paseo Companeros
   Chico, CA 95928

7. Ron R. and Nancy E. Piret.....2
   567 Paseo Companeros
   Chico, CA 95928

8. Commander.....1
   Naval Oceanography Command
   Stennis Space Center, MS 39529-5000